Chapter 11
Structure-Function Relationships in the Mn_4CaO_5 Water-Splitting Cluster

Jian-Ren Shen

Abstract Mn_4CaO_5 cluster is the catalytic center for photosynthetic water-splitting harbored in photosystem II (PSII), a huge, multi-subunit membrane–protein complex located in the thylakoid membranes from cyanobacteria to higher plants. The structure of PSII has been analyzed at 1.9 Å resolution by X-ray crystallography, revealing a clear picture of the Mn_4CaO_5 cluster. In this chapter, principles of crystallization and crystal structure analysis are briefly introduced, followed by descriptions of the structure of the Mn_4CaO_5 cluster and its implications in the mechanism of water-splitting. Based on the geometric organization of the Mn_4CaO_5 cluster, the location of four terminal water ligands, the possible oxidation states of the four Mn ions reported so far, as well as the structural changes revealed by replacing the Ca ion with Sr, a mechanism for water-splitting was proposed and discussed.

Keywords Photosystem II • Oxygen evolution • Crystal structure • Photosynthesis • Membrane proteins • Crystallization • S-state

Abbreviations

DFT	Density functional theory
EM	Electron microscopy
EPR	Electron paramagnetic resonance
EXAFS	Extended X-ray absorption fine structure
FTIR	Fourier transform infrared spectroscopy

J.-R. Shen, Ph.D. (✉)
Photosynthesis Research Center, Graduate School of Natural Science and Technology, Okayama University, Tsushima Naka 3-1-1, Kita-ku, Okayama 700-8530, Japan
e-mail: shen@cc.okayama-u.ac.jp

J. Golbeck and A. van der Est (eds.), *The Biophysics of Photosynthesis*, Biophysics for the Life Sciences 11, DOI 10.1007/978-1-4939-1148-6_11,

NMR Nuclear magnetic resonance
OEC Oxygen-evolving complex
PSII Photosystem II

11.1 Introduction

Photosynthetic water-splitting is catalyzed by a Mn_4CaO_5 cluster, which is harbored in photosystem II (PSII), a large, multi-subunit membrane protein complex located in the thylakoid membranes of all oxygenic photosynthetic organisms [1]. The splitting of water using the energy from the sunlight produces electrons, protons, and molecular oxygen. While the former two products are the sources of energy required for the synthesis of ATP by the ATP synthase and reducing power, both are necessary for the fixation of carbon dioxide into carbohydrates, the latter product is indispensable for sustaining the oxygenic life on the earth. Thus, the photosynthetic water-splitting is one of the most important biochemical reactions occurring on the earth.

In order to understand the mechanism of water-splitting, it is essential to elucidate the structure of the Mn_4CaO_5 cluster and its surrounding protein environment. The main methods for solving the structure of biomacromolecules are X-ray crystallography, nuclear magnetic resonance (NMR), and electron microscopy (EM). X-ray crystallography is the most powerful method for structure determination of biomacromolecules, while the NMR method is subjected to limitations in molecular masses that can be treated, and the structures of very few proteins have been solved at an atomic resolution by the EM method. Since PSII is a large membrane–protein complex, (for example, the typical PSII core complex with a full oxygen-evolving activity from cyanobacteria contains 20 different subunits with a total molecular mass of 350 kDa, see Chapters 1–3 in [1, 2]), the only way available to analyze the structure of this type of huge protein complexes at an atomic detail is X-ray crystallography.

The basic procedure for X-ray crystallography is protein sample preparation, crystallization, diffraction data collection, phase determination, electron density analysis, model building, and refinement. The most important and also the most difficult step in X-ray crystallography is obtaining a single crystal with a good quality and reasonably high resolution. Owing to remarkable technical and methodological advances in recent years, it has become rather easy to obtain crystals of soluble proteins. However, getting well-diffracted single crystals of membrane proteins still remains a major obstacle and a rate-limiting step in solving their structures by X-ray crystallography. This is especially true for large, multi-subunit membrane–protein complexes such as PSII. Once a well-diffracted single crystal is obtained, obtaining phase information necessary for calculation of the electron density map can sometimes be a time-consuming task; however, there are several alternative methods to solving this problem now, so that in most cases this will not present a major obstacle.

In the following, the principles of protein crystallization and X-ray structure analysis are briefly described, followed by introduction and discussions on the structure and function of the oxygen-evolving complex (OEC) of PSII that have been revealed from the structural and functional analyses of PSII.

11.2 Crystallization of Soluble and Membrane Proteins

11.2.1 Principles of Protein Crystallization

Protein crystals are ordered arrays of a single, homogeneous protein, or a complex of multiple proteins. Because the quality and resolution of a crystal depend on the degree of ordering of the protein molecules within the crystal, a highly purified, homogeneous protein or protein complex preparation is a prerequisite for getting a high quality crystal. The homogeneity of a protein or a protein complex is evaluated from a number of different properties of the protein in question, among them, the main ones include the absence of contaminating components, a homogeneous net total charge, and a homogeneous size distribution of the protein particles in solution. While the former one is easily evaluated from electrophoresis, the latter two are more difficult to be determined. To determine whether the protein of interest is homogeneous in charge distribution, one can usually use ion-exchange column chromatography, isoelectric point electrophoresis, etc. To determine the homogeneity of size distribution, conventional size-exclusion chromatography can be used along with dynamic light-scattering measurement, various native polyacrylamide electrophoresis, etc.

Various factors can influence the purity and homogeneity of a protein solution, since even a single protein may adopt slightly different, multiple conformations in solution due to influences of various factors such as salts and/or other chemicals, redox reagents, detergents, temperature, pH, etc. Thus, not only exclusion of other protein components is important for getting a good start for crystallization, keeping the protein conformation as uniform as possible is also extremely important. Another factor to be considered is the stability of the protein in solution, since in most cases the process of crystallization takes several days to several weeks at 4 °C to room temperature; in many cases, purified protein cannot sustain such a long time without losing its active conformation. This is especially important for membrane proteins and their complexes, since membrane proteins are crystallized in the presence of detergents (see below), the stability of most membrane proteins will be reduced in the presence of detergents.

In principle, crystallization is achieved by bringing a protein solution into a supersaturated state, so that the protein molecules exceeding the saturation concentration can no more be dissolved and will be partitioned into an aggregated phase. The supersaturated state can be divided into three phases [3, 4]: one is a metastable phase where proteins can still exist in the solubilized form despite that

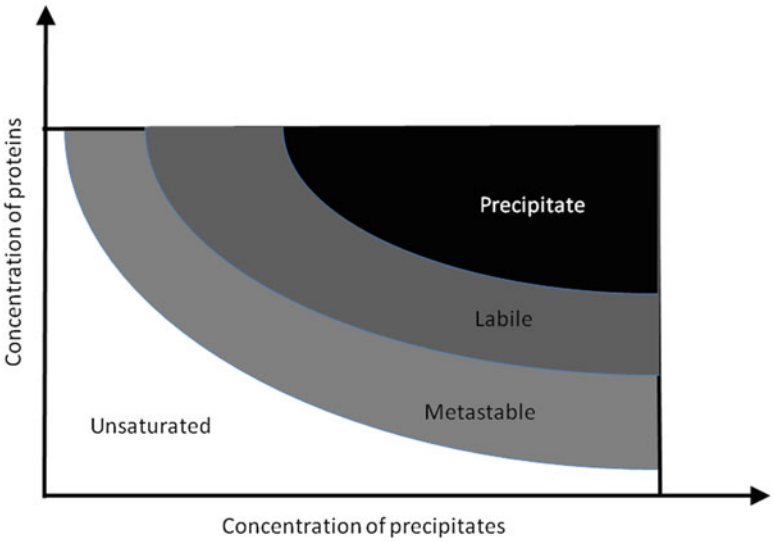

Fig. 11.1 Phase diagram. The concentration of proteins is plotted against increased concentrations of precipitates, but it can be other factors such as temperature, pH, etc. Saturation level increases as the color goes from *white* to *black*. The *white* region represents unsaturated solutions where crystals will dissolve. The supersaturated region can be divided further into three regions, namely the metastable phase where only crystal growth will occur, the labile phase where nucleation and growth compete, and the precipitate region which has the highest supersaturation and precipitation of amorphous protein will occur in this region

its concentration already exceeds (slightly) the saturation concentration; the second one is a labile phase which has a higher degree of saturation where the crystal nuclei can be formed; and the third one is a precipitation phase where the supersaturation reaches a high level that enables the solutes (proteins) to precipitate immediately (Fig. 11.1). The nuclei of crystals formed in the labile phase can grow in either the labile phase or metastable phase. The labile phase will give a faster growth of the crystals, whereas the metastable phase results in a slower growth due to lower degree of supersaturation. In general, slower growth of crystals is preferred to ensure the quality and resolution of the crystals to be obtained, since faster growth of the crystals will bring more chances of occurrence of disorders in the crystal packing due to increases in the occurrence of errors caused by the fast attachment of new protein molecules into the already existed small crystals, resulting in imperfect arrangement of the protein molecules in the crystal. This means that a lower degree of supersaturation such as in the metastable state will facilitate the growth of high quality crystals. In practice, however, the degree of supersaturation is not easy to control, and it is determined by experience in most cases. A slower growth rate means that a longer time is needed to obtain the crystals, which will require enough stability of the protein under the conditions employed, a requirement to be found often difficult to be met by certain proteins. Thus, the choice of growth rate for

crystals depends on the balance between the stability of the protein in question and the quality of the crystal to be obtained.

In order to bring a protein solution into a supersaturated state, various "precipitants" are used; these include various salts, polymers (the typical one is polyethylene glycols (PGEs)), and even organic solvents. For the success of crystallization, not only the type and concentration of the precipitants but also a number of other factors need to be considered; these include the pH of the solution (type of buffer used), salts and redox reagents co-existed, temperature, additives etc., in addition to the purity and homogeneity of the protein samples used. The process of crystallization is therefore to find an appropriate condition that enables the separation of protein molecules into an ordered array from a supersaturated solution while preventing the formation of precipitants and random aggregation [5–7]. It is noticed, however, that the crystallization often occurs in the interface between solution and aggregation, so that appearance of some aggregation is inevitable in some cases. High quality crystals, on the other hand, are usually obtained in the best growth conditions where no aggregation will be observed.

11.2.2 Methods of Protein Crystallization

A number of methods have been developed to bring a protein solution into a supersaturated state [5–7]. The most widely used ones are batch crystallization, vapor diffusion, and dialysis methods. In the batch (or micro-batch) method, a protein solution is mixed with a precipitant solution to bring it to a supersaturated state, which is then covered with a layer of oil to prevent evaporation. The mixed solution is allowed to stay for a few hours to a few days during which the crystals are formed. In the micro-batch method used recently, the mixed protein solution layer is covered by a layer of paraffin oil which allows water molecules to pass through very slowly, enabling a slow evaporation to occur to enhance the degree of supersaturation. The batch method is easy to use and set up, so can be used for screening a large number of different conditions. Due to the constancy or small change in the degree of supersaturation during the entire process of crystallization, however, the batch method is used for the formation of crystals only in a narrow range of precipitant concentration as well as other conditions.

Vapor diffusion is the most widely used method for crystallization in which a protein solution is mixed with typically an equal volume of a precipitant solution. The mixed protein solution is still unsaturated, which is then spotted into a sealed chamber where a large excess volume of the precipitant solution is included. The water will evaporate from the protein solution toward the precipitant solution, bringing the protein solution to the supersaturated state during the course of evaporation. Depending on the setup of the protein and precipitant solutions, the vapor diffusion method can be divided into hanging drop, sitting drop, and sandwich drop methods. Evaporation of water molecules enables relatively a large change in the concentration of both protein and other components; thus, vapor

diffusion allows screening of relatively a large range of conditions among which crystals may be formed. Vapor diffusion is also easy to use and set up, and is thus suitable for screening a large number of conditions.

The dialysis method uses a dialysis membrane to separate the protein solution and the precipitant solution. During the crystallization process, the precipitant can enter into the protein solution, and the water molecules can also go out from the protein solution to the precipitant solution, reaching equilibrium between the two solutions. This method allows the control of the final composition of the protein solution by controlling the composition of the precipitant solution; however, the setup of this method is often time-consuming so that it is often not suitable for screening a large number of conditions which are required for the initial screening of crystallization for a novel protein.

11.2.3 Crystallization of Membrane Proteins

Crystallization of membrane proteins and their complexes resembles that of soluble proteins, but membrane proteins have large areas of hydrophobic surfaces, which make them insoluble in water. Thus, membrane proteins need proper detergents for their solubilization, purification, and stabilization, which make the purification and crystallization of membrane proteins more difficult than soluble proteins. The most commonly used detergents for membrane proteins are those of nonionic detergents, as they appear to be most mild in solubilizing membrane proteins. Detergents form micelles in solution, which will surround the membrane proteins to ensure their solubilization in aqueous solutions. The concentrations needed to form micelles (critical micelle concentration, CMC) are largely different among different types of detergents. The choice of a proper detergent for the success of crystallization of a particular membrane protein or membrane protein complex, however, appears not easy, as the detergent needs to be in proper interaction not only with the membrane protein but also with the other components in the crystallization solution [8, 9]. Another issue is that, a detergent suitable for the solubilization and purification of a membrane protein may not be suitable for formation of a high quality crystal; thus, the detergent needs to be changed for crystallization after purification. The addition of detergents to the crystallization conditions dramatically increases the number of conditions that need to be screened; this is one of the major reasons why membrane proteins are more difficult to be crystallized in addition to the hydrophobic nature of them that hinders crystallization.

In the practice of membrane protein crystallization, addition of small, amphiphilic molecules was often found to improve the crystals, which are assumed to fill in the spaces in the crystal packing that are not occupied by detergents and protein amino acid residues [8, 9]. In addition, a unique approach to utilize the hydrophobic nature of membrane proteins for crystallization was also developed, which is the lipid cubic phase method. In this method, a cubic phase is formed by a high concentration of lipids (usually monoolein) which enables the membrane proteins

to be incorporated to form an ordered array [10–12]. Another approach that has been used successfully in crystallization of some membrane proteins is to reduce the hydrophobic surface of a membrane protein and increase its hydrophilic surface by binding of monoclonal antibody fragments [13], or by fusion with a soluble protein such as T4 lysozyme [14, 15], so that the membrane protein can be crystallized in a way more like a soluble protein.

11.3 X-ray Structure Analysis

In the conventional optical microscopy, visible light is used to visualize small objects not directly visible by eyes. In order to do so, light reflected from the small objects is collected and magnified by suitable lenses at a proper distance from the objects. The resolution, or the smallest distance of two points that can be identified, by this method, is limited by the wavelength of the light used, since the resolution cannot be significantly higher than the wavelength of the light used, which is in the range of 400–700 nm for the visible light. To reveal the atomic structure of molecules, X-ray at wavelengths of around 1 Å has to be used, since a typical distance for a C–C bond is around 1.5 Å. Due to the high energy of X-rays, however, no suitable lenses are available to collect and magnify the X-rays; thus, an alternative method employing calculations must be used.

A crystal is made up of identical, basic units arranged equally in all directions in the space (Fig. 11.2a). The repeated unit of a crystal is called "unit cell," and its properties are defined by three lengths *a*, *b, c*, along the x, y, z directions, as well as three angles α, β, γ, between each pair of the axes (Fig. 11.2b). These values constitute the unit cell parameters, which are different among different types of

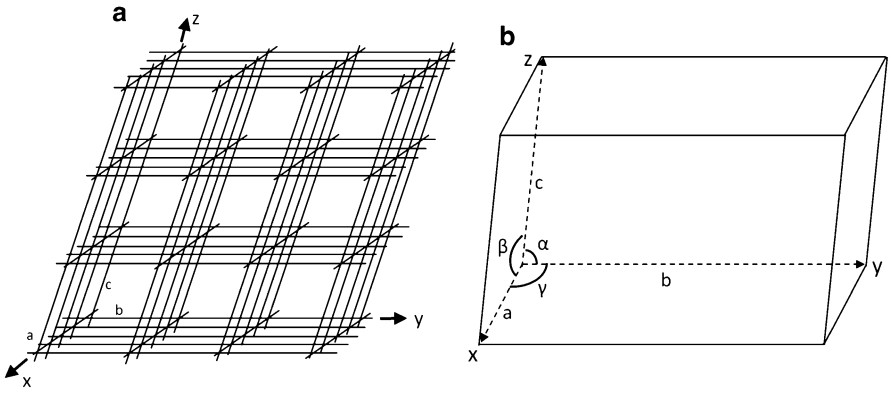

Fig. 11.2 Schematic representation of crystal packing and a unit cell of a crystal. (**a**) Schematic representation of a region of a crystal, where identical units are arranged in exactly the same way. (**b**) A unit cell from a crystal, showing the definition of six parameters that define the symmetry and properties of the crystal

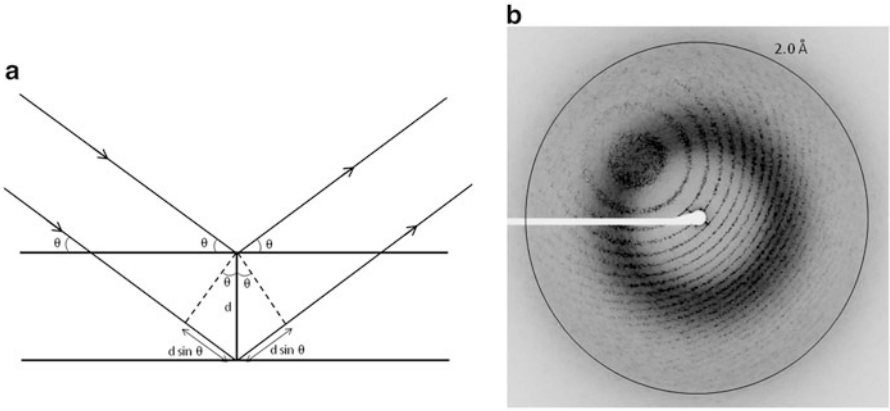

Fig. 11.3 Occurrence of diffraction from crystallographic planes and an example of diffraction pattern. (**a**) The crystal can be considered to consist of a series of planes, each of which scatter the incident wave. Two such crystal planes were shown here. The difference between the scattered waves from these two planes is the difference in the pathlength between these planes, which equals 2d sinθ. When this path difference equals a multiple of the wavelength, the waves add constructively and a diffraction peak is observed. (**b**) An example of diffraction pattern, taken from a crystal of oxygen-evolving photosystem II core complex. The *circle* represents the resolution point of 2.0 Å

crystals, and their relationship is related with the symmetry of the crystal. The arrangement of the unit cells constitutes the lattice of the crystal, and there are 14 lattices (Bravais lattices) that are allowed for protein crystals [16–18].

When an incident X-ray hits an object, the electrons of atoms in the object were forced to oscillate, generating a second X-ray having the same energy (wavelength) as that of the incident X-ray (Thomson Scattering). This second X-ray is scattered from every atom constituting the object, and can be captured at a distance much longer than the inter-atom distances behind the object. If the object is a crystal, that is, an ordered array of identical units, then the "diffracted" X-rays are summed up in some places but canceled out in other places, giving rise to visible (detectable) "diffraction spots." This is the phenomenon of interference of multiple waves with the same wavelength. To illustrate this, we consider that the incident wave (X-ray) hits two planes of atoms in a crystal with an angle of θ (Fig. 11.3a). The path difference between the two waves scattered from the two planes at the same angle θ is "2d sinθ," where *d* is the distance between the two planes. Diffraction spot is observed only when the path difference is equal to a multiple of the wavelength according to:

$$2d\ \sin\theta = n\lambda$$

where *n* is an integer. This is the Bragg's law that determines whether a diffraction spot can be observed or not from a crystal. From this relationship, one can easily deduce that the maximum value of *d*, that is, the largest distance between two adjacent layers in the crystal that can yield diffraction, is given by:

$$d = \lambda/2$$

This is the theoretical limit of resolution with a given wavelength λ. In practice, this limit of resolution is rarely achieved with protein crystals due to various imperfections existed within the crystals.

The diffraction pattern (see Fig. 11.3b for an example) is determined by the arrangement of atoms in the repeated units within the crystal; in other words, the amplitude and position of every diffraction spot in the diffraction pattern contain information regarding the arrangement of atoms (species and position of the atoms) within the crystal. Thus, the diffraction patterns can be used to determine the molecular structure of the crystal. The relationship between the diffraction pattern and molecular structure, however, is reciprocal, and the diffraction pattern can be considered to represent the molecular structure in a reciprocal space relative to the molecular structure in the real space [16–18]. This relationship is related by a mathematical treatment Fourier transform; thus, the molecular structure in the crystal can be deduced from the diffraction pattern by the method of Fourier transform, and vice versa. During this treatment, however, the phase information of the X-ray wave that yielded the diffraction pattern is lost, so that it has to be determined separately by another method [16–18]. This is the phase problem in protein crystallography.

Several methods have been developed to solve the phase problem, among which the most traditional one is the multiple isomorphous replacement (MIR) method. In this method, crystals are soaked with metal (heavy atom) compounds, and the diffraction pattern is measured and compared with native crystals without metals bound. This gives rise to the position of the metals bound to the protein crystal, which is then used to calculate the phase information. The second method utilizes multiple anomalous dispersion (MAD) from a single metal, in which diffraction pattern is measured with several wavelengths around the transition energy of the metal bound to the protein. Since each metal has a characteristic absorption wavelength in the X-ray region, the differences in the diffraction measured around this specific wavelength are primarily contributed by the electrons of that metal, which is thus used for locating the position of the metal and for generating the initial phase information. The third method is the molecular replacement (MR) method, which utilizes a known structure of a homologous protein as the initial search model. All of the above methods have been widely used, with the latter two becoming increasingly popular owing to the availability of intense, tunable X-rays from synchrotron radiation facilities and a number of atoms with anomalous scattering capability, as well as the increasing number of solved structures.

Because the diffraction of X-rays is caused by electrons of atoms, the results calculated from the diffraction pattern are distributions of electrons in a three-dimensional space, or an electron density map. The molecular structure is then built by fitting amino acid residues and ligands into the electron density map, which is the process of model building. In order to obtain the model that best fits with the experimentally obtained electron density map, the model initially obtained is refined against the experimental data through many cycles of refinement until reaching a state that gives a minimum difference between the experimentally obtained electron density map and model. During this refinement process,

knowledge of stereochemistry such as constraints in the configuration of amino acids and their spatial conflicts in the three-dimensional structure of the protein is incorporated to minimize the model errors.

The quality of the structures obtained from the X-ray crystallography is determined by a number of factors, among which the most important one is the resolution which in turn depends on the degree of order of molecules in the crystal. A higher resolution represents a more accurate, reliable structure than a lower resolution. A higher resolution will also give a lower value of R factor, a parameter related to the reliability of the structure, as well as a lower average temperature factor (*B*-factor).

11.4 Crystal Structure Analysis of PSII

PSII is an integral membrane protein complex found in the thylakoid membranes from prokaryotic cyanobacteria to higher plants. The composition of PSII core capable of oxygen evolution varies slightly from cyanobacteria to higher plants. In the cyanobacterial PSII whose structure has been solved at an atomic resolution, there are 17 transmembrane subunits and 3 peripheral, hydrophilic subunits, which gives rise to a total molecular mass of 350 kDa [1, 2]. The purified PSII, especially those from thermophilic cyanobacteria, exists predominately in a dimeric form [19–21], which is thought to be also the functional form dominant in vivo.

Since PSII is an extremely large membrane–protein complex, its structure has to be solved by X-ray crystallography. The large, membranous nature of the complex also presented a major challenge to obtain high resolution crystals of PSII. The first crystal structure of PSII was reported by Zouni and colleagues in 2001 at a resolution of 3.8 Å, from a thermophilic cyanobacterium *Thermosynechococcus elongatus* [21]. The use of the thermophilic cyanobacterium enabled them to obtain a highly stable, active PSII core dimer preparation as was already shown previously [22, 23]. In this structure, the position of major PSII subunits was assigned in a Cα model, together with the position of the Mn_4Ca cluster that catalyzes the water-splitting reaction. The side chain structures of amino acids and positions of some small subunits were not given due to the limited resolution. Subsequently, Kamiya and Shen reported a 3.7 Å structure of PSII dimer from a closely related thermophilic cyanobacterium *Thermosynechococcus vulcanus*, in which a few more subunits were assigned, together with some residues with their side chains assigned [24]. However, the structure of the Mn_4Ca cluster was still not clear, since each of the metal atoms and the presumed oxo-bridges connecting the metal atoms were not separated in the electron density map, making the electron density of the metal cluster like a ball packed with all of the five metal ions and possible oxo-bridges. The resolution of the PSII structure was raised to 3.5 Å [25], 3.0 Å [26], and 2.9 Å resolutions [27] gradually, which continuously improved the structure of the whole complex in terms of the side chain orientations of amino acid residues, a number of

cofactors such as chlorophylls, carotenoids, lipids, a bicarbonate ion, etc. The presence of Ca^{2+} as an integral part of the water-oxidizing catalyst was demonstrated by a number of biochemical and biophysical studies including EPR and EXAFS measurements, and its global position in the Mn_4Ca cluster was first identified in the 3.5 Å structure from anomalous scattering at a wavelength near the Ca absorption edge [25], which was confirmed subsequently by the higher resolution structures [26, 27]. However, the detailed structure of the Mn_4Ca cluster, as well as its exact ligand environment, the position of water molecules, etc., remained obscure even in the 2.9 Å structure. In fact, the electron density for the Mn_4Ca cluster was still a ball encapsulating all of the metal ions and oxo-bridges, and the electron densities for each of the atoms were not separated, so that the position of the individual atoms cannot be clearly determined from the experimentally obtained electron density, and the structural model has to incorporate constraints from previous results mainly from extended X-ray absorption fine structure (EXAFS) measurements and electron paramagnetic resonance (EPR) studies.

The atomic structure of the PSII dimer complex was reported in 2011 by Shen and his colleagues at a resolution of 1.9 Å [28]. At this resolution, the electron densities for the individual atoms in the Mn_4Ca cluster were clearly separated, allowing determination of the structure of the metal cluster unambiguously. In addition, the structure revealed the coordination environment of the metal cluster in much more detail than the previously obtained structure, as well as the presence of a huge number of water molecules associated with various residues in the PSII dimer. In the following, we describe the structure of PSII at the atomic resolution, with the focus on the detailed structure of the Mn_4Ca cluster, and its functional implications in the mechanism of water-splitting.

11.4.1 Overall Structure of the PSII Dimer

The overall structure of PSII dimer analyzed at the 1.9 Å resolution is shown in Fig. 11.4a, which contains 19 subunits per monomer, among which 16 are transmembrane subunits and 3 are membrane peripheral subunits required for oxygen evolution. Among the transmembrane subunits of PSII, D1 and D2 subunits have five transmembrane helices each and form the reaction center of PSII to which most of the electron transfer cofactors are bound. Two other large transmembrane subunits are CP47 and CP43 (CP stands for chlorophyll protein), which have six transmembrane helices each and are located in the two sides of the D1/D2 core. These two subunits bind a large number of chlorophylls (17 for CP47 and 12 for CP43) which function as light-absorbing antenna chlorophylls to transfer the light energy to the reaction center chlorophylls. In addition to these large transmembrane subunits, 12 small subunits (with molecular mass less than 10 kDa) were found, most of them have one transmembrane helix and only PsbZ has two transmembrane helices. These give rise to a total of 35 transmembrane helices for a PSII monomer.

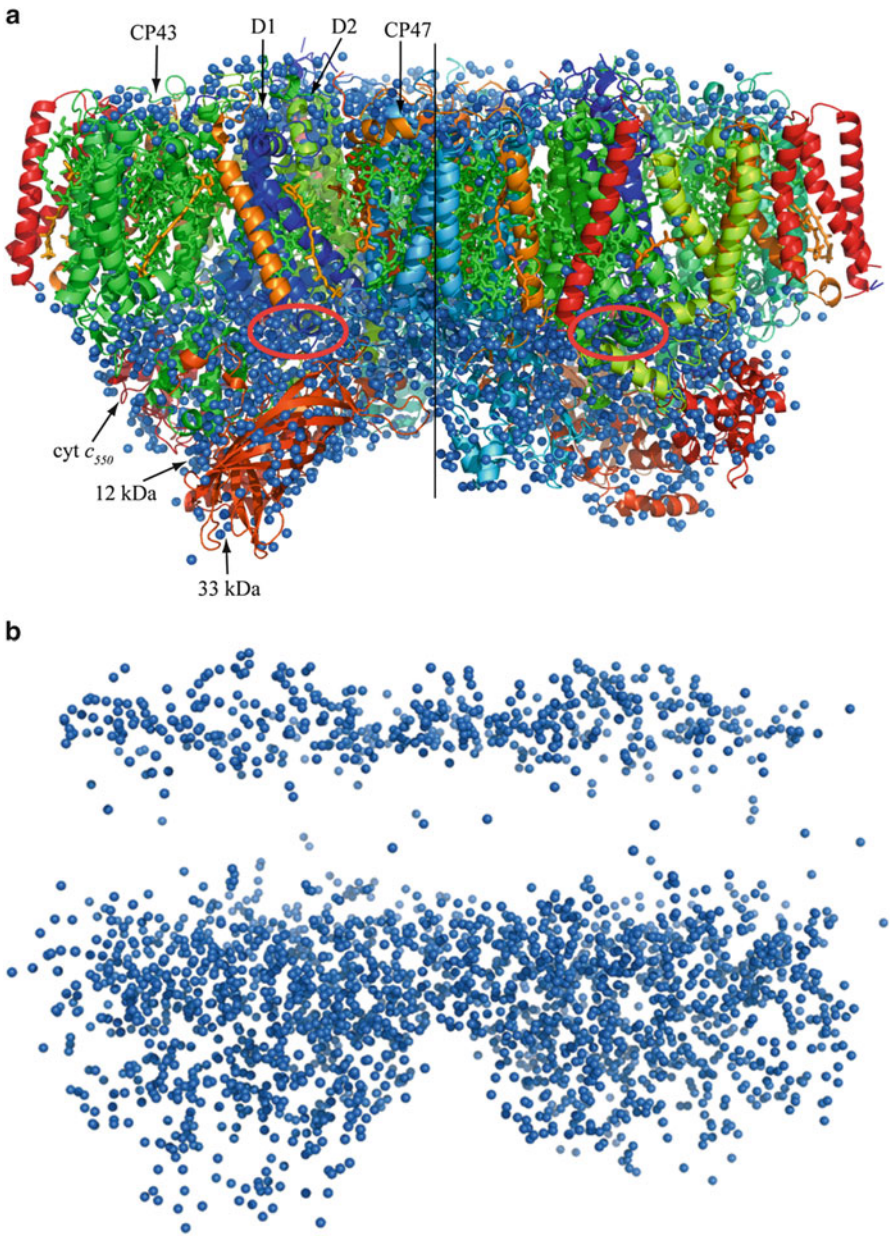

Fig. 11.4 Overall structure of PSII dimer. (**a**) Overall structure of a PSII dimer analyzed at 1.9 Å resolution. View from a direction perpendicular to the membrane normal. The *line* in the middle represents the non-crystallographic twofold axis dividing the two monomers, and the two *red circles* indicate the region where the water-splitting catalytic center, the Mn_4CaO_5 cluster, binds. (**b**) Distribution of the water molecules. All of the protein and cofactors except water were removed from panel (**a**), showing the distribution of water molecules in the PSII dimer

PsbY, one of the low molecular mass of PSII with one single transmembrane helix located in the peripheral region close to PsbE and PsbF (the α- and β-subunits of cytochrome b559), was not present in the crystal structure, indicating that it is lost during crystallization due to its weak association with the PSII core complex.

The three peripheral, hydrophilic subunits are PsbO (33 kDa), PsbV (cytochrome *c550*), and PsbU (12 kDa), located in the lumenal side of the thylakoid membrane. They form a cap for the site of oxygen evolution (the Mn_4CaO_5 cluster), shielding it from the bulk solution with a large area of hydrophilic protein region. These extrinsic proteins have been shown to be important for maintaining the activity and stability of the oxygen-evolving complex (OEC).

In addition to the protein subunits, 35 chlorophylls, 2 pheophytins, 11 β-carotenes, 2 plastoquinones, 1 bicarbonate, 1 *b*-type and 1 *c*-type cytochromes, 1 non-heme iron, more than 20 lipid molecules, at least 2 chlorides, a Mn_4CaO_5 cluster, etc., are present in a PSII monomer.

One of the most significant features of the high resolution structure of PSII was the presence of a huge number of water molecules within it. In total, nearly 2,800 water molecules were found in a PSII dimer; these water molecules were distributed in two layers, one in the surface of the cytoplasmic (stromal) side and the other one in the surface of the lumenal side, of the thylakoid membrane (Fig. 11.4b). Very few water molecules were found in the transmembrane region. These distribution of the water molecules demonstrates a typical feature for a membrane protein complex. The few water molecules present in the transmembrane region were found to serve as ligands or hydrogen-bonding partners of chlorophylls that are not ligated by an amino acid residue. Typically, the Mg ion of the chlorin ring of chlorophylls is ligated by an amino acid residue; in most cases it is a His residue. Among the 35 chlorophylls in a PSII monomer, however, 7 chlorophylls do not have an amino acid residue as a ligand for its Mg ion. Instead, it is ligated by a water molecule [28]. For such chlorophylls that are ligated by water, there are usually two additional water molecules existing in the vicinity of the chlorin ring and form hydrogen bonds to the carbonyl groups of the chlorin ring as well as the direct water ligand, which are probably required to stabilize the chlorin ring not directly ligated to an amino acid residue.

11.4.2 Structure of the Mn_4CaO_5 Cluster

The Mn_4CaO_5 cluster is bound in a pocket formed by residues of D1 and CP43 in the lumenal surface of the thylakoid membrane (cycled regions in Fig. 11.4a). Because the interatomic distances within the cluster is in the range of 1.7–2.6 Å, it is not possible to separate each of the atoms in the crystal structures up to 2.9 Å resolution. At these low resolutions, the electron density for the whole cluster is connected, making it look like a pear-shaped ball (or a soccer ball), so that the placement of individual atoms within the ball was not possible based on the experimentally

obtained electron density map only [21, 24–27]. Early models of the metal cluster was thus built with the constrains obtained from other approaches, notably from EXAFS experiments. The results of EXAFS experiments have suggested that there should be 2–3 Mn–Mn distances of 2.7–2.8 Å, as well as some longer distances in the range of 3.0–3.3 for Mn–Mn and Mn–Ca [29–34]. These distances were used to place the Mn and Ca atoms within the electron density of the pear-shaped ball albeit with no clear separation of the electron density for the individual atoms. An even worse situation was seen for oxo-bridges, which must be present in order to connect the Mn–Mn and Mn–Ca pairs and have been suggested also from EXAFS experiments. Since Mn and Ca have much more electrons than those of oxygen atoms, the diffracted X-rays by these metal ions are much stronger than that diffracted by oxygens. Thus, the electron density forming the pear-shaped ball at lower resolutions is largely contributed by the Mn and Ca ions, and the densities contributed by oxygen atoms are very weak, making the assignment of oxo-bridges essentially impossible at low resolutions.

In the 1.9 Å resolution structure of PSII [28], the electron densities for each of the metal ions, together with the oxo-bridged oxygens, were clearly separated, allowing the assignment of each atom unambiguously (Fig. 11.5a). As a result, the catalytic center for water oxidation was found to contain five oxygen atoms in addition to four Mn and one Ca ions, forming a Mn_4CaO_5 cluster (Fig. 11.5b). Since the number of electrons of Mn (with a valence of III or IV) is three or four larger than that of Ca (II), the electron density of the Ca ion is slightly lower than those of the Mn ions (Fig. 11.5a). This is also an illustration for the quality of the electron density obtained at the atomic resolution, as the slight differences in the intensity of the electron density between Mn and Ca ions are not easy to be distinguished at a lower resolution. The core of the cluster is a distorted cubane made up by three Mn ions (Mn1–Mn3), four oxygen atoms (O1–O3, and O5), and one Ca ion. The fourth Mn (Mn4) is located outside of the cubane and connected to the cubane core by two oxo-bridges via O4 and O5. The shape of the whole cluster resembles that of a distorted chair, with the cubane serving as the chair base and the outside Mn (Mn4) serving as the back of the chair (Fig. 11.5c).

The distorted shape represents one of the most significant features of the Mn_4CaO_5 cluster structure, that is, the instable or flexible nature of the metal complex (see below for further discussions). The distortion is mainly caused by two reasons. One is the differences in the Mn–O distances. Among the five oxygen atoms, O1–O4 have bond distances to their nearby Mn ions in the range of 1.8–2.2 Å, which is similar to those typically found in Mn oxide compounds. The distances between O5 and its nearby Mn ions, however, were found to be extremely longer in the crystal structure, namely 2.4, 2.5, 2.6 Å for O5–Mn3, O5–Mn4, and O5–Mn1, respectively. These distances, in particular the O5–Mn4, O5–Mn1 distances, are much longer than those expected for normal Mn oxides, suggesting a weak binding of the O5 atom to the nearby Mn ions (see below for more detailed discussions). The other reason that contributed to the distortion in the structure of the Mn_4CaO_5 cluster is the differences between typical Mn–O and Ca–O distances.

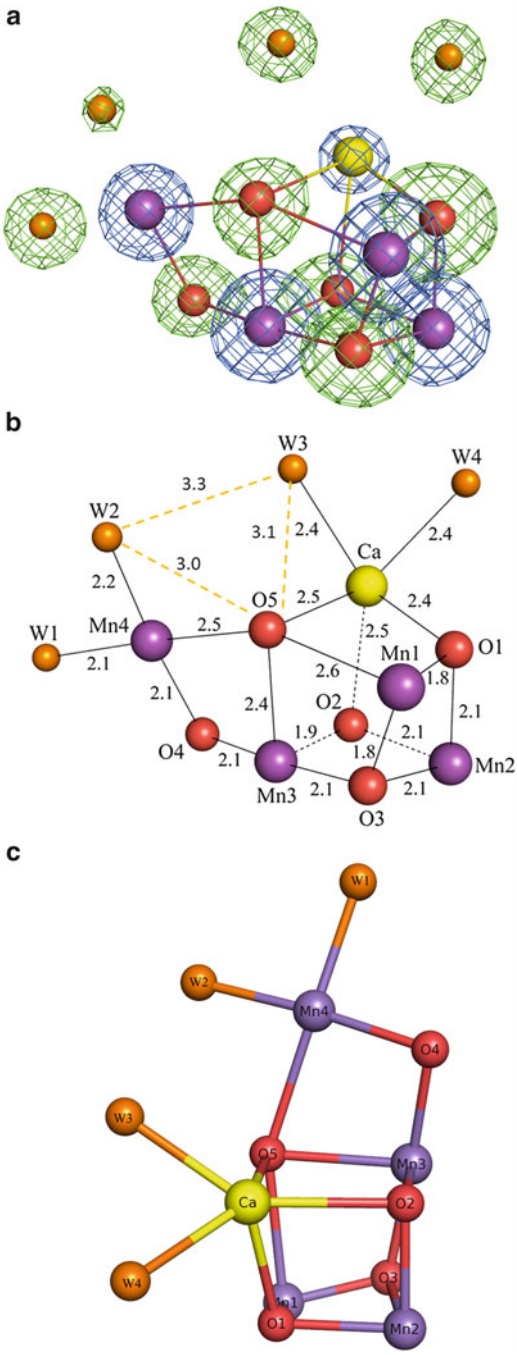

Fig. 11.5 Structure of the Mn_4CaO_5 cluster. (**a**) Individual atoms of the Mn_4CaO_5 cluster, superimposed with the 2Fo-Fc map (*blue*) contoured at 5σ for manganese and calcium atoms, and with the omit map (*green*) contoured at 7σ for oxygen atoms and water molecules. (**b**) Bond distances (in Å) between metal ions and oxo-bridges or water molecules within the Mn_4CaO_5 cluster. (**c**) Distorted chair form of the Mn_4CaO_5 cluster. The structure of the cluster was rotated relative to that shown in (**b**), to show the chair form more clearly

As described above, while the typical Mn–O distances are in the range of 1.8–2.2 Å, the typical distances of Ca–O are in the range of 2.4–2.6 Å due to a lower positive charge of the Ca ion compared with that of Mn ions. The incorporation of the only Ca ion in the metal cluster therefore contributed to the distorted shape of the structure, which may be important for the flexibility or catalytic activity of the catalytic core.

In addition to the oxo-bridged oxygens, four water molecules are associated with the Mn_4CaO_5 cluster as terminal ligands [28]. These water ligands are designated W1–W4, among which two (W1 and W2) are associated with Mn4, whereas the other two (W3, W4) are associated with the Ca ion (Fig. 11.5). Interestingly, no other direct water ligands were found to associate with the remaining three Mn ions, indicating that the region formed by Mn4, Ca, and the four water molecules is highly hydrophilic, and may play an important role in water-splitting. Among these four water molecules, W2 bound to Mn4, and W3 bound to Ca, are in hydrogen-bonding distances to O5. Furthermore, W2 and W3 are also within a hydrogen-bond distance with each other. These suggested that the area formed by W2, W3, and O5 may constitute the site of O–O bond formation during the water-splitting reaction (see below for further discussions).

The distances of the two water ligands to Mn4 are 2.1–2.2 Å, whereas those between W3 and W4 to Ca are 2.4 Å. The slightly shorter distances between water and Mn4 reflect a higher valence of Mn4 than that of the Ca ion, and thus a slightly stronger binding of the water ligands to Mn4 than those to the Ca ion.

11.4.3 Comparison of Mn–Mn and Mn–O Distances Between the Crystal Structure and EXAFS Studies and Theoretical Calculations

The shortest distances between Mn ion pairs are 2.8 Å for Mn1–Mn2, 2.9 Å for Mn2–Mn3, and 3.0 Å for Mn3–Mn4 in the 1.9 Å resolution crystal structure. These distances are slightly longer than the distances reported from EXAFS experiments, where it was suggested that there are at least two Mn–Mn distances of 2.7–2.8 Å [29, 30, 35], and a third one at 2.8 Å may also be present [31, 33, 34, 36]. While these differences may fall within the experimental errors, as the results of crystal structure analysis at 1.9 Å resolution bear an average error of 0.16 Å for the interatomic distances [28], theoretical calculations using the coordinates of the crystal structure have been performed to examine the Mn–Mn as well as Mn–O distances. Extensive quantum mechanical/molecular mechanical (QM/MM) calculations using the coordinates of the crystal structure have resulted in model structures for the Mn_4CaO_5 cluster where the shortest Mn–Mn distances resemble those of EXAFS results but slightly shorter (0.1–0.2 Å) than those of the crystal structure [37–45]. This has been taken as evidence to indicate that the crystal structure is in a reduced

state than that of the S_1-state presumed in the X-ray structural analysis. While this possibility cannot be excluded at present due to possible X-ray radiation damage, there is another source of difference that needs to be considered. Since in the X-ray structure analysis at 1.9 Å resolution, the hydrogen atom cannot be assigned, so that the four terminal water ligands have been assumed as H_2O, and the five oxo-bridged oxygens have been assigned as O^{2-}. It is possible that the protonation states of some of the water molecules and/or oxo-bridges are different from those assumed in the crystal structure, and the exact combination of the protonation states is not known at present. A combination of the protonation states different from the real structure may affect the results of theoretical calculations.

More profound differences were found in the distances of Mn1–O5 and Mn4–O5 between the crystal structure and theoretical calculations. As described above, both of the distances between Mn1 and O5, and between Mn4 and O5, are unusually long, which were never obtained in theoretical calculations if the O5 atom is in an O^{2-} form. Assuming that O5 is in a deprotonated state (O^{2-}), theoretical calculations yielded a result showing that the distance between Mn4 and O5 is in the range of 1.8–2.3 Å, whereas that between Mn1 and O5 is in the range of 2.8–3.3 Å [37–45]. This suggests that the O5 atom is bonded to Mn4 but not to Mn1; therefore Mn4 is 6-coordinated whereas Mn1 is 5-coordinated in the S_1-state (see below for more detailed discussions). This is remarkably different from that of the crystal structure, where O5 sits in nearly the middle between Mn4 and Mn1, and suggested that it is weakly bonded to both Mn4 and Mn1, resulting in a quasi-five-coordinated structure for both Mn4 and Mn1 in the S_1-state. The term "quasi-five-coordinated" is used to indicate that the sixth ligand is at a distance apparently longer than the usual Mn–O distance. The unusually longer distances between O5–Mn4 and O5–Mn1 may again caused by the possible radiation damage during X-ray data collection. However, when O5 is assumed to be in a protonated state, namely, an OH^- form, a DFT calculation yielded Mn4–O5 and Mn1–O5 distances that are rather close to the crystal structure [39]. This suggests that O5 may be in a protonated state. Alternatively, theoretical calculations performed so far may have not incorporated the protein environment surrounding the Mn_4CaO_5 cluster in an area large enough to account the precise structure of the cluster. In any cases, the unusual position of O5 is consistent with the above discussions that the area around O5 may form the reaction site for water-splitting and O–O bond formation.

11.4.4 Ligand Environment of the Mn_4CaO_5 Cluster

The Mn_4CaO_5 cluster is coordinated by seven amino acids, among which six are carboxylate residues and one is a His residue (Fig. 11.6a) [28]. The six carboxylate residues are D1-D170, D1-E189, D1-E333, D1-D342, D1-A344, and CP43-E354,

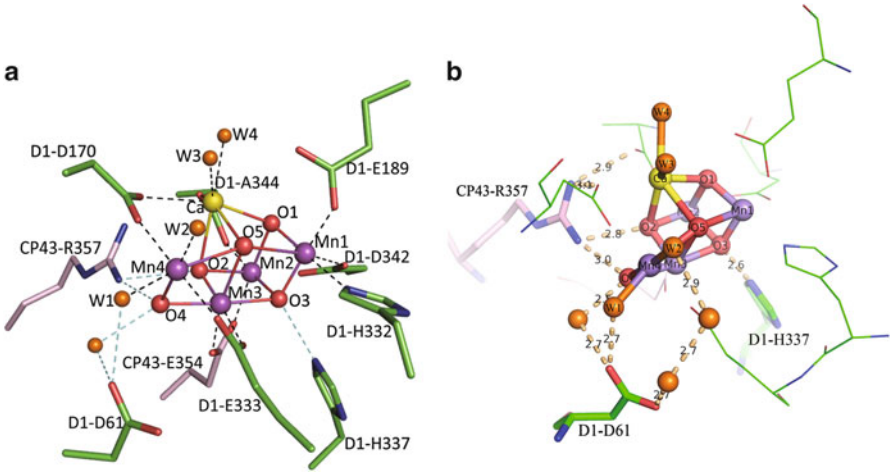

Fig. 11.6 Ligand environment of the Mn_4CaO_5 cluster. (**a**) Direct ligands to the Mn_4CaO_5 cluster. (**b**) Three residues, namely D1-D61, D1-H337, and CP43-R357, that form hydrogen bonds to the oxo-bridged oxygens in the Mn_4CaO_5 cluster

Table 11.1 Ligands for each of the metal ions in the Mn_4CaO_5 cluster of PSII

Atom	Ligands	Atom	Ligands	Atom	Ligands	Atom	Ligands	Atom	Ligands
Mn1	O1	Mn2	O1	Mn3	O2	Mn4	O4	Ca	O1
	O3		O2		O3		O5		O2
	O5		O3		O4		D170A		O5
	E189A		D342A		O5		E333A		D170A
	H332A		A344A		E333A		W1		A344A
	D342A		E354C		E354C		W2		W3
									W4

among which five are bi-dentate ligands and only D1-E189 is a mono-dentate ligand to Mn1. D1-A344 is the C-terminal residue of the D1 subunit, and two additional residues D1-E333 and D1-D342 are located in the C-terminal of the D1 subunit, illustrating that the C-terminal region of the D1 subunit is heavily involved in maintaining the structure of the Mn_4CaO_5 cluster. The only His residue is D1-H332, which is ligated to Mn1. These ligands, together with the oxo-bridges and terminal water ligands, constitute the saturated ligand environment for the Mn_4CaO_5 cluster. As a result, all of the four Mn ions are 6-coordinated (see above discussions for Mn4 and Mn1), and the Ca ion is 7-coordinated (Table 11.1).

In addition to the direct ligands to the Mn_4CaO_5 cluster, most of which are negatively charged; three residues are located close to the cluster and form hydrogen bonds with one or more of the oxo-bridged oxygens. These three residues are CP43-R357, D1-H337, and D1-D61 (Fig. 11.6b), and they are either positively charged, neutral or negatively charged. Among these three residues, CP43-R357 forms hydrogen bonds to both O2 and O4, D1-H337 forms a hydrogen bond to O3,

whereas D1-D61 is connected to O4 by hydrogen bond via a water molecule. These hydrogen bonds may be important to maintain the distorted, flexible structure of the Mn_4CaO_5 cluster. If we assume that no hydrogen bonds are present for the oxygen atoms, the O–Mn bonds in the cluster would have distances similar to those found in typical Mn oxides, which are in the range of 1.8–2.2 Å. These short distances will yield a rigid, un-distorted structure of the cluster difficult to undergo structural changes accompanying the S-state transitions. In other words, the "flexibility" expected from the distorted structure of the metal cluster will be lost, which would yield a compound with little or no catalytic activity for water-splitting. It is thus the distorted chair form, or the flexibility, of the Mn_4CaO_5 cluster that is most important for the water-splitting activity. Photosynthetic organisms have gained this "instable" structure through a long time of evolution, and have maintained this structure for even a longer time from the advent of prokaryotic cyanobacteria some 2.7 billion years ago to higher plants we see today.

11.4.5 Effects of Sr^{2+} Substitution for Ca^{2+} on the Structure of the Mn_4CaO_4 Cluster

Since the only Ca ion in the Mn_4CaO_5 cluster can be easily removed without destroying the overall structure of the cluster, and its removal completely diminishes oxygen evolution, its role in oxygen evolution has been studied extensively [46–50]. From the structural features of the Mn_4CaO_5 cluster revealed at the atomic resolution [28], one of the roles of the Ca ion appears to introduce the distortion into the structure as mentioned above. We can easily imagine that if the cluster is made up with Mn and O atoms only, its structure would become symmetric and hardly be distorted, and the resulted compound will become a rigid, stable one unable to undergo structural changes. This happens to most artificially synthesized Mn–O compounds, which are rigid, stable, and with no or low catalytic activity. Introduction of a Ca ion into Mn–O compounds has been successful in some cases; however, the position of the Ca ion is not exactly the same as that found in the native Mn_4CaO_5 cluster, so that no artificially synthesized Mn–Ca–O compounds have been obtained that match the catalytic activity of the native cluster.

Another important role that might be expected for the Ca ion, and that was implied from the crystal structure, is the binding of substrate water molecule. In the crystal structure, two water molecules were found to associate with the Ca ion; one of these two water molecules may thus function as one of the substrate water for O–O bond formation. In order to explore this possibility, the Ca was replaced with Sr, and the resulted Sr-substituted PSII was used for crystallization and crystal structural analysis [51]. Sr^{2+} is the only divalent ion capable of supporting water-splitting with an activity half of Ca-containing PSII. Thus, slight structural changes are expected by replacing Ca^{2+} with Sr^{2+}, which may be responsible for the decrease in oxygen evolution. The structure of Sr-substituted PSII was analyzed

at a resolution of 2.1 Å, which showed several small differences in the Mn–O and Sr–O distances compared with that of the Mn_4CaO_5 cluster [51]. The most significant difference, however, was found in the bond distance between Sr and one of the water ligands, W3, which became 2.6 Å, a distance 0.2 Å longer than the corresponding distance in the Mn_4CaO_5 cluster. On the other hand, the distance between W4 and Sr became 2.3 Å, which is largely similar with the corresponding distance (2.4 Å) in the Mn_4CaO_5 cluster. These results suggest that W3 binds to Ca^{2+} more weakly than W4, and is thus more mobile than W4. In fact, the position of W3 was found to be moved by 0.5 Å in the Sr^{2+}-substituted PSII relative to that in the native PSII [51]. This implies that W3 may have a higher reactivity than W4, which further implies that W3 may be involved in the water-splitting and O–O bond formation.

11.4.6 Possible Mechanisms of O–O Bond Formation

Water oxidation proceeds through the S-state cycle [52–54], where four photons are absorbed to drive sequential removal of four electrons from the Mn_4CaO_5 cluster, leading to the successive accumulation of four oxidizing equivalents in the metal cluster. The removal of electrons is accompanied by release of protons, which typically has a pattern of 1, 0, 1, 2 for the S_0–S_1, S_1–S_2, S_2–S_3, and S_3–(S_4)–S_0 transitions [55, 56]. The S_0, S_1-states are dark stable, whereas S_2, S_3-states are unstable at room temperature, and the S_4-state is highly unstable that has not been trapped stably under normal (room temperature and normal oxygen pressure) conditions. The O–O bond formation occurs during the S_3–(S_4)–S_0 transition.

The oxidation states of the four Mn ions in the S_1-state are believed to be in a combination of (III, III, IV, IV) based on EPR (ENDOR) studies on the mulitline signal characteristic of the S_2-state [57–61], as well as FXAFS studies [33, 35], although a lower oxidation state has been proposed that can also explain the experimental data [40, 62]. The oxidation states of the individual Mn ions in the S_1 and S_2-states, however, have not been assigned unambiguously. It has been reported that Mn1, the only Mn ion to which an amino acid ligand other than a carboxylate group (D1-His332) is associated, is 5-coordinated in the S_2-state, suggesting that it is in a valance of III (3+) in the S_2-state [63]. If this is the case, this Mn ion must be III also in the S_1-state. The other Mn that has a valence of III in the S_1-state is not clear; no experimental evidence relating to this Mn has been obtained. As described above, the specific O5 is sitting in the middle between Mn1 and Mn4 in the crystal structure, and both distances of O5 to Mn1 and Mn4 are exceptionally longer compared to typical Mn–O distances found in Mn oxide. This suggests that both Mn1 and Mn4 have a weak sixth ligand, implying that they are not fully 6-coordinated. The long bonding distances between Mn1 and Mn4 to O5 can be explained by a large Jan-Teller distortion that Mn(III) possesses, which is in support of the notion that Mn1 is III in the S_1-state. This in turn implies that Mn4 is also III in the S_1-state.

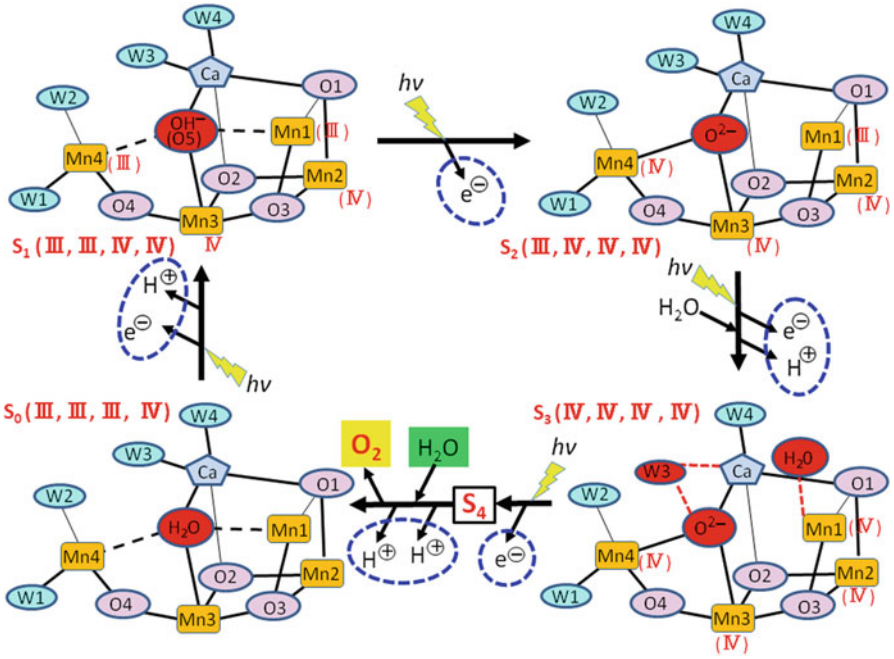

Fig. 11.7 A possible mechanism of water-splitting and O–O bond formation based on the atomic structure of the Mn_4CaO_5 cluster. See text for detailed discussions

Based on these considerations, as well as the discussions described above that the O–O bond formation may occur in the area formed by W2, W3, and O5, we may propose a mechanism for the formation of water-splitting and O–O bond formation, which is illustrated in Fig. 11.7. In this proposed mechanism, the Mn_4CaO_5 cluster has a (III, III, IV, IV) valence combination in the S_1-state, with the Mn4 and Mn1 in the III form, and Mn2 and Mn3 in the IV form. In this state, the O5 is assumed to be an OH^- species based on its long distances and thus weak binding to Mn1 and Mn4. Upon transition from S_1 to S_2 by absorption of one photon, one electron is removed from Mn4, leading to a IV state of Mn4. Due to this change, the binding of O5 to Mn4 becomes stronger than that to Mn1, resulting in a movement of O5 toward Mn4. This results in a "full" 6-coordinates for Mn4, whereas breaks the bond between O5 and Mn1, yielding a 5-coordinated Mn1 in the S_2-state, as has been suggested previously. No protons are released during this transition, and the possible structural changes may be small due to the removal of only one electron from S_1-to-S_2 transition.

In the subsequent transition from S_2 to S_3, one electron and one proton are removed. The electron may be removed from the only 3+ Mn ion remained, which is Mn1, resulting in a Mn(IV) species in the Mn1 site. This Mn1 will require to be 6-coordinated, which may be fulfilled by insertion of a new water ligand during this transition. Indeed, the insertion of a water molecule has been suggested from Fourier

transform infrared (FTIR) spectroscopic experiments [64, 65]. On the other hand, the proton may be released from the O5 site (which was assumed to be an OH^- species in the S_2-state), resulting in an O^{2-} species in this state. These changes may result in a large structural rearrangement of the whole cluster, which has been suggested from previous FTIR, EXAFS, and EPR experiments [35, 47, 49, 57, 59, 66]. One presumed consequence of this structural rearrangement may be a move of the position of W3 toward O5, resulting in a closer distance between these two species, or even already a formation of the "pseudo-double bond" of O–O between these two species.

In the S_3–(S_4)–S_0 transition, one electron and two protons are removed, accompanied by an insertion of a new water molecule. The two protons may be removed from W3, or one from W3 and one from another species, which may reinforce the O–O bond formed between W3 and O5. These changes finally force the breakage of bonds between W3 and Ca, as well as those between O5 and nearby metals, thereby release one O_2 molecule. The O_5 position may be occupied by the newly inserted water molecule in the S_0-state, from which one proton is removed during the transition from S_0 to S_1. This completes one cycle of the water oxidation reaction.

It should be pointed out that the above proposed mechanism is one of the possible mechanisms for water oxidation, and there are other possibilities that cannot be excluded at present. For example, the O–O bond formation may occur between W2 and W3 without the involvement of O5, or even between O5 and a newly inserted water molecule bound to Mn1 as proposed by Siegbahn [67, 68], since Mn1 has a 5-coordinated structure and may be actively involved in the structural rearrangements during the S-state transitions. Answers to the real mechanism for water oxidation may not be obtained until the structural rearrangements occurred during the S-state transitions are elucidated.

11.4.7 Hydrogen-Bond Networks and Proton Channels

During the S-state transitions, four protons must be removed. Since the Mn_4CaO_5 cluster is embedded deeply in the PSII protein matrix covered by a large area formed by thee hydrophilic, extrinsic subunits, as well as the membrane-extrinsic loops of large transmembrane subunits CP47, CP43, D1, and D2 [28], there must be channels for the exit of protons outside of the catalytic site to the lumenal bulk solution as well as channels for the inlet of substrate water molecules. In the atomic structure of PSII, there are indeed a number of well-defined hydrogen-bond networks connecting the Mn_4CaO_5 cluster to the lumenal surface of the PSII protein complex, which may function as proton exit channels or water inlet channels [27, 28, 69–71].

One example of such channels is mediated by Y_Z, an electron mediator between the Mn_4CaO_5 cluster and the PSII reaction center chlorophylls. Y_Z has been identified to be Tyr161 of the D1 subunit, and a well-defined hydrogen-bond network was found between D1-Tyr161 and the Mn_4CaO_5 cluster [28]. This network

extends further from D1-Tyr161 to the lumenal bulk phase. First, D1-Tyr161 is hydrogen-bonded to the two water molecules coordinated to Ca either directly (W4) or indirectly (W3) through another water (Fig. 11.8a). The hydrogen bond between the additional water and D1-Tyr161 that mediates the link from W3 to Tyr161 has a length of 2.6 Å, suggesting that this is a strong (low barrier) hydrogen bond [28, 72]. This additional water also mediates the hydrogen bond between the two water molecules bound to Mn4 and D1-Tyr161. On the other hand, another strong hydrogen bond was found between D1-Tyr161 and the ε-nitrogen of D1-His190, which has a distance of 2.5 Å and is in the opposite side of the Mn_4CaO_5 cluster. D1-His190 was further hydrogen-bonded to D1-Asn298 and to several water molecules and amino acid residues including CP43-Ala411, D1-Asn322, and PsbV-Tyr137, leading to an exit pathway to the lumenal bulk solution (PsbV-Tyr137 is the C-terminal residue of the PsbV subunit) (Fig. 11.8a) [28]. This hydrogen-bond network is located in the interfaces between D1, CP43, and PsbV subunits, and may function as an exit channel for protons that arise from proton-coupled electron transfer (PCET) via Y_Z. This is in support of the existence of a PCET pathway involving D1-Tyr161 and D1-His190 as suggested previously [73–75]. PsbV-Tyr137 at the exit of this channel is surrounded by several charged residues including D1-Arg323, D1-His304, and PsbV-Lys129; these residues may therefore function to regulate the proton excretion through the PCET pathway.

Another example of the hydrogen-bond network starts from one of the ligands to the Mn_4CaO_5 cluster, D1-E333, and mediated by D1-D61 and Cl-1 [28]. Cl-1 is one of the two chloride binding sites found in PSII, which are located in two sides of the Mn_4CaO_5 cluster and have distances of 6–7 Å to the Mn_4CaO_5 cluster [76, 77]. Cl-1 is surrounded by D1-K317, D1-E333, and two water molecules. The hydrogen-bond network extends from D1-D61 and Cl-1 through several amino acid residues and water molecules formed by the interfaces of D2, PsbO, and CP47, to the surface of the protein complex in the lumenal bulk solution (Fig. 11.8b). This hydrogen-bond network may function for the exit of protons or inlet of water molecules. In fact, both D1-D61 and Cl-1 have been suggested to be important for the activity of oxygen evolution from either mutagenesis [78] or Cl-depletion studies [79, 80].

11.5 Concluding Remarks and Future Perspectives

The geometric structure of the Mn_4CaO_5 cluster has been revealed from the structural analysis of PSII at an atomic level, which made PSII the largest membrane protein whose structure was solved beyond 2.0 Å resolution. Although there are still some debates regarding the bond distances of Mn–Mn and Mn–O in the crystal structure probably due to possible radiation damages, the mechanism of water oxidation and O–O bond formation could be considered based on the current structure where a huge number of water molecules are revealed. The exact reaction mechanism and the structural rearrangements possibly occurring during the S-state

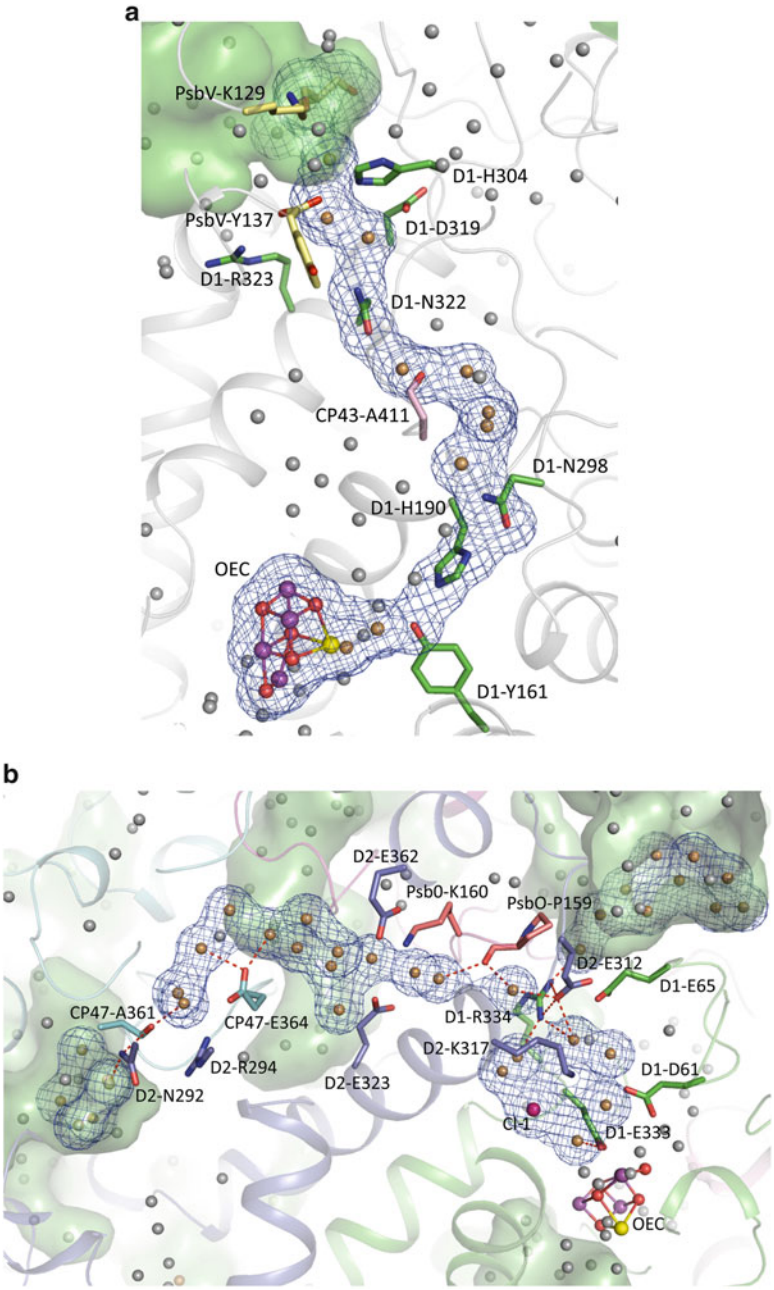

Fig. 11.8 Examples of hydrogen-bond networks found in the atomic resolution structure of PSII. (**a**) A hydrogen-bond network mediated by Y_Z, D1-Tyr161. The network starts from the water molecules hydrogen-bonded to Ca, through D1-Tyr161, several water molecules and amino acid residues, and finally exits to the lumenal bulk solution through PsbV-K129. The *green* area in the *upper left* side represents lumenal solution phase. (**b**) Hydrogen-bond network mediated by Cl-1. The network starts from one of the ligand to the Mn_4CaO_5 cluster D1-E333, through Cl-1, D1-D61, several water molecules and amino acid residues, and exits to the lumenal solution. The *green* regions represent lumenal solution phase

transitions, however, have to be determined until some, or all, of the structures of the intermediate S-states can be obtained. This will be greatly benefited by the use of the high resolution crystals already obtained, as well as a combination of various advanced biophysical techniques such as X-ray absorption spectroscopy, advanced EPR techniques, and FTIR. These spectroscopic techniques may yield unique information regarding the structures, dynamics, and oxidation states of the catalytic site. In addition, the availability of X-ray free electron lasers (XFEL) is worth to be mentioned in particularly, since it provides ultra-short pulses (fs) of intense X-rays which may allow diffraction data to be collected free of radiation damage (a principle so-called diffraction before explosion), as well as data collection from shortly lived intermediate states. Elucidation of the water-splitting mechanism will be important for the designing of artificial catalyst capable of splitting water using the energy from the sun, a source of ultimate clean energy for powering life on the earth.

Acknowledgements Structural analysis of PSII at the atomic resolution described in this chapter was performed in collaboration with Drs. Nobuo Kamiya, Yasufumi Umena, and Keisuke Kawakami, and analysis of the Sr-PSII was performed in collaboration with Dr. Faisal H.M. Koua in addition to the above colleagues. I thank these colleagues for their continuous contributions. The work performed in the author's laboratory is supported by a Grant-in-Aid for Specially Promoted Research from MEXT/JSPS of Japan.

References

1. Wydrzynski TJ, Satoh K, editors. Photosystem II, The light-driven water:plastoquinone oxidoreductase. Dordrecht, The Netherlands: Springer; 2005.
2. Shen JR, Henmi T, Kamiya N. Structure and function of photosystem II. In: Fromme P, editor. Photosynthetic protein complexes. A structural approach. Weinheim: Wiley-VCH Verlag GmbH & Co. KGaA; 2008. p. 83–106.
3. Li M, Chang WR. Protein crystallization. Photosynth Res. 2009;102:223–9.
4. Weber PC. Overview of protein crystallization methods. Macromol Crystallogr A. 1997;276:13–22.
5. Bergfors TM, editor. Protein crystallization: techniques, strategies, and tips. San Diego, CA: International University Line (IUL); 1999.
6. Chayen NE, Saridakis E. Protein crystallization: from purified protein to diffraction-quality crystal. Nat Methods. 2008;5:147–53.
7. McPherson A. Crystallization of biological macromolecules. New York, NY: Cold Spring Harbor Laboratory Press; 1999.
8. Michel H, editor. Crystallization of membrane proteins. Boca Raton, FL: CRS press; 1990.
9. Iwata S, editor. Methods and results in crystallization of membrane proteins. San Diego, CA: International University Line (IUL); 2003.
10. Caffrey M, Cherezov V. Crystallizing membrane proteins using lipidic mesophases. Nat Protoc. 2009;4:706–31.
11. Katona G, Andréasson U, Landau EM, et al. Lipidic cubic phase crystal structure of the photosynthetic reaction centre from *Rhodobacter sphaeroides* at 2.35 Å resolution. J Mol Biol. 2003;331:681–92.
12. Landau EM, Rosenbusch JP. Lipidic cubic phases: a novel concept for the crystallization of membrane proteins. Proc Natl Acad Sci U S A. 1996;93(25):14532–5.

13. Hunte C, Michel H. Crystallization of membrane proteins mediated by antibody fragments. Curr Opin Struct Biol. 2002;12:503–8.
14. Cherezov V, Rosenbaum DM, Hanson MA, Rasmussen SG, Thian FS, Kobilka TS, Choi HJ, Kuhn P, Weis WI, Kobilka BK, Stevens RC. High-resolution crystal structure of an engineered human β2-adrenergic G protein-coupled receptor. Science. 2007;318:1258–65.
15. Rosenbaum DM, Cherezov V, Hanson MA, Rasmussen SG, Thian FS, Kobilka TS, Choi HJ, Yao XJ, Weis WI, Stevens RC, Kobilka BK. GPCR engineering yields high-resolution structural insights into β2-adrenergic receptor function. Science. 2007;318:1266–73.
16. Allen JP, Seng C, Larson C. Structures of proteins and cofactors: X-ray crystallography. Photosynth Res. 2009;102:231–40.
17. Drenth J. Principles of protein X-ray crystallography. New York, NY: Springer; 1999.
18. Chayen NE, Helliwell JR, Snell EH. Macromolecular crystallization and crystal perfection. Oxford: Oxford University Press; 2010.
19. Kuhl H, Kruip J, Seidler A, Krieger-Liszkay A, Bunker M, Bald D, Scheidig AJ, Rogner M. Towards structural determination of the water-splitting enzyme. Purification, crystallization, and preliminary crystallographic studies of photosystem II from a thermophilic cyanobacterium. J Biol Chem. 2000;275:20652–9.
20. Shen JR, Kamiya N. Crystallization and the crystal properties of the oxygen-evolving photosystem II from *Synechococcus vulcanus*. Biochemistry. 2000;39:14739–44.
21. Zouni A, Witt HT, Kern J, Fromme P, Krauß N, Saenger W, Orth P. Crystal structure of photosystem II from *Synechococcus elongatus* at 3.8 Å resolution. Nature. 2001;409:739–43.
22. Shen JR, Inoue Y. Binding and functional properties of two new extrinsic components, cytochrome *c*550 and a 12 kDa protein, in cyanobacterial photosystem II. Biochemistry. 1993;32:1825–32.
23. Sugiura M, Inoue Y. Highly purified thermo-stable oxygen-evolving photosystem II core complex from the thermophilic cyanobacterium *Synechococcus elongatus* having His-tagged CP43. Plant Cell Physiol. 1999;40:1219–31.
24. Kamiya N, Shen JR. Crystal structure of oxygen-evolving photosystem II from *Thermosynechococcus vulcanus* at 3.7-Å resolution. Proc Natl Acad Sci U S A. 2003;100:98–103.
25. Ferreira KN, Iverson TM, Maghlaoui K, Barber J, Iwata S. Architecture of the photosynthetic oxygen-evolving center. Science. 2004;303:1831–8.
26. Loll B, Kern J, Saenger W, Zouni A, Biesiadka J. Towards complete cofactor arrangement in the 3.0 Å resolution structure of photosystem II. Nature. 2005;438:1040–4.
27. Guskov A, Kern J, Gabdulkhakov A, Broser M, Zouni A, Saenger W. Cyanobacterial photosystem II at 2.9 Å resolution and role of quinones, lipids, channels and chloride. Nat Struct Mol Biol. 2009;16:334–42.
28. Umena Y, Kawakami K, Shen JR, Kamiya N. Crystal structure of oxygen-evolving photosystem II at a resolution of 1.9 Å. Nature. 2011;473:55–60.
29. Dau H, Liebisch P, Haumann M. The structure of the manganese complex of photosystem II in its dark-stable S_1-state: EXAFS results in relation to recent crystallographic data. Phys Chem Chem Phys. 2004;6:4781–92.
30. Dau H, Grundmeier A, Loja P, Haumann M. On the structure of the manganese complex of photosystem II: extended-range EXAFS data and specific atomic resolution models for four S-states. Philos Trans R Soc Lond B. 2008;363:1237–44.
31. Pushkar Y, Yano J, Glatzel P, Messinger J, Lewis A, Sauer K, Bergmann U, Yachandra V. Structure and orientation of the Mn_4Ca cluster in plant photosystem II membranes studied by polarized range-extended X-ray absorption spectroscopy. J Biol Chem. 2007;282:7198–208.
32. Sauer K, Yano J, Yachandra VK. X-ray spectroscopy of the photosynthetic oxygen-evolving complex. Coord Chem Rev. 2008;252:318–35.
33. Yano J, Kern J, Sauer K, Latimer MJ, Pushkar Y, Biesiadka J, Loll B, Saenger W, Messinger J, Zouni A, Yachandra VK. Where water is oxidized to dioxygen: structure of the photosynthetic Mn_4Ca cluster. Science. 2006;314:821–5.

34. Zein S, Kulik LV, Yano J, Kern J, Pushkar Y, Zouni A, Yachandra VK, Lubitz W, Neese F, Messinger J. Focusing the view on nature's water-splitting catalyst. Philos Trans R Soc Lond B. 2008;363:1167–77.
35. Haumann M, Müller C, Liebisch P, Iuzzolino L, Dittmer J, Grabolle M, Neisius T. Meyer-KlauckeW, Dau H. Structural and oxidation state changes of the photosystem II manganese complex in four transitions of the water oxidation cycle (S_0/S_1, S_1/S_2, S_2/S_3, and S_3, S_4/S_0) characterized by X-ray absorption spectroscopy at 20 K and room temperature. Biochemistry. 2005;44:1894–908.
36. Yano J, Pushkar Y, Glatzel P, Lewis A, Sauer K, Messinger J, Bergmann U, Yachandra VK. High-resolution Mn EXAFS of the oxygen-evolving complex in photosystem II: structural implications for the Mn_4Ca cluster. J Am Chem Soc. 2005;127:14974–5.
37. Ames W, Pantazis DA, Krewald V, Cox N, Messinger J, Lubitz W, Neese F. Theoretical evaluation of structural models of the S_2 state in the oxygen evolving complex of photosystem II: protonation states and magnetic interactions. J Am Chem Soc. 2011;133:19743–57.
38. Grundmeier A, Dau H. Structural models of the manganese complex of photosystem II and mechanistic implications. Biochim Biophys Acta. 2012;1817:88–105.
39. Isobe H, Shoji M, Yamanaka S, Umena Y, Kawakami K, Kamiya N, Shen JR, Yamaguchi K. Theoretical illumination of water-inserted structures of the $CaMn_4O_5$ cluster in the S_2 and S_3 states of oxygen-evolving complex of photosystem II: full geometry optimizations by B3LYP hybrid density functional. Dalton Trans. 2012;41:13727–40.
40. Petrie S, Gatt P, Stranger R, Pace RJ. Modelling the metal atom positions of the photosystem II water oxidising complex: a density functional theory appraisal of the 1.9 angstrom resolution crystal structure. Phys Chem Chem Phys. 2012;14:11333–43.
41. Siegbahn PEM. The effect of backbone constraints—the case of water oxidation by the oxygen evolving complex in photosystem II. ChemPhysChem. 2011;12:3274–80.
42. Siegbahn PE. Water oxidation mechanism in photosystem II, including oxidations, proton release pathways, O–O bond formation and O_2 release. Biochim Biophys Acta. 2013;1827 (8–9):1003–19. doi:10.1016/j.bbabio.2012.10.006.
43. Yamaguchi K, Isobe H, Yamanaka S, Saito T, Kanda K, Shoji M, Umena Y, Kawakami K, Shen JR, Kamiya N, Okumura M. Full geometry optimizations of the mixed-valence $CaMn_4O_4X(H_2O)_4$ (X = OH or O) cluster in OEC of PS II: degree of symmetry breaking of the labile Mn-X-Mn bond revealed by several hybrid DFT calculations. Int J Quan Chem. 2013;113:525–41.
44. Yamaguchi K, Yamanaka S, Isobe H, Saito T, Kanda K, Umena Y, Kawakami K, Shen JR, Kamiya N, Okumura M, Nakamura H, Shoji M, Yoshioka Y. The nature of chemical bonds of the $CaMn_4O_5$ cluster in oxygen evolving complex of photosystem II: Jahn-Teller distortion and its suppression by Ca doping in cubane structures. Int J Quan Chem. 2013;113:453–73.
45. Luber S, Rivalta I, Umena Y, Kawakami K, Shen JR, Kamiya N, Brudvig GW, Batista VS. S_1-state model of the O_2-evolving complex of photosystem II. Biochemistry. 2011;50:6308–11.
46. Boussac A, et al. Biosynthetic Ca^{2+}/Sr^{2+} exchange in the photosystem II oxygen-evolving enzyme of *Thermosynechococcus elongatus*. J Biol Chem. 2004;279:22809–19.
47. Cox N, et al. Effect of Ca^{2+}/Sr^{2+} substitution on the electronic structure of the oxygen-evolving complex of photosystem II: a combined multifrequency EPR, ^{55}Mn-ENDOR, and DFT study of the S_2 state. J Am Chem Soc. 2011;133:3635–48.
48. Ishida N, et al. Biosynthetic exchange of bromide for chloride and strontium for calcium in the photosystem II oxygen-evolving enzymes. J Biol Chem. 2008;283:13330–40.
49. Pushkar Y, Yano J, Sauer K, Boussac A, Yachandra VK. Structural changes in the Mn_4Ca cluster and the mechanism of photosynthetic water splitting. Proc Natl Acad Sci U S A. 2008;105:1879–84.
50. Suzuki H, Taguchi Y, Sugiura M, Boussac A, Noguchi T. Structural perturbation of the carboxylate ligands to the manganese cluster upon Ca^{2+}/Sr^{2+} exchange in the S-state cycle of photosynthetic oxygen evolution as studied by flash-induced FTIR difference spectroscopy. Biochemistry. 2006;45:13454–64.

51. Koua FHM, Umena Y, Kawakami K, Shen JR. Structure of Sr-substituted photosystem II at 2.1 Å resolution and its implications in the mechanism of water oxidation. Proc Natl Acad Sci U S A. 2013;110:3889–94.
52. Dau H, Haumann M. The manganese complex of photosystem II in its reaction cycle—basic framework and possible realization at the atomic level. Coord Chem Rev. 2008;252:273–95.
53. Joliot P. Period-four oscillations of the flash-induced oxygen formation in photosynthesis. Photosynth Res. 2003;76:65–72.
54. Kok B, Forbush B, McGloin M. Cooperation of charges in photosynthetic oxygen evolution. I. A linear four step mechanism. Photochem Photobiol. 1970;11:457–75.
55. Junge W, Haumann M, Ahlbrink R, Mulkidjanian A, Clausen J. Electrostatics and proton transfer in photosynthetic water oxidation. Philos Trans R Soc Lond B. 2002;357:1407–18.
56. Suzuki H, Sugiura M, Noguchi T. Monitoring proton release during photosynthetic water oxidation in photosystem II by means of isotope-edited infrared spectroscopy. J Am Chem Soc. 2009;131:7849–57.
57. Britt RD, Campbell KA, Peloquin JM, Gilchrist ML, Aznar CP, Dicus MM, Robblee J, Messinger J. Recent pulsed EPR studies of the photosystem II oxygen-evolving complex: implications as to water oxidation mechanisms. Biochim Biophys Acta. 2004;1655:158–71.
58. Kulik LV, Epel B, Lubitz W, Messinger J. ^{55}Mn pulse ENDOR at 34 GHz of the S_0 and S_2 states of the oxygen-evolving complex in photosystem II. J Am Chem Soc. 2005;127:2392–3.
59. Kulik LV, Epel B, Lubitz W, Messinger J. Electronic structure of the Mn_4OxCa cluster in the S_0 and S_2 states of the oxygen-evolving complex of photosystem II based on pulse ^{55}Mn-ENDOR and EPR spectroscopy. J Am Chem Soc. 2007;129:13421–35.
60. McEvoy JP, Gascon JA, Batista VS, Brudvig GW. The mechanism of photosynthetic water splitting. Photochem Photobiol Sci. 2005;4:940–9.
61. Peloquin JM, Campbell KA, Randall DW, Evanchik MA, Pecoraro VL, Armstrong WH, Britt RD. ^{55}Mn ENDOR of the S_2-state multiline EPR signal of photosystem II: implications on the structure of the tetranuclear Mn cluster. J Am Chem Soc. 2000;122:10926–42.
62. Kolling DR, Cox N, Ananyev GM, Pace RJ, Dismukes GC. What are the oxidation states of manganese required to catalyze photosynthetic water oxidation? Biophys J. 2012;103:313–22.
63. Stich TA, Yeagle GJ, Service RJ, Debus RJ, Britt RD. Ligation of D1-His332 and D1-Asp170 to the manganese cluster of photosystem II from *Synechocystis* assessed by multifrequency pulse EPR spectroscopy. Biochemistry. 2011;50:7390–404.
64. Noguchi T. FTIR detection of water reactions in the oxygen-evolving centre of photosystem II. Philos Trans R Soc Lond B Biol Sci. 2008;363:1189–94.
65. Suzuki H, Sugiura M, Noguchi T. Monitoring water reactions during the S-state cycle of the photosynthetic water-oxidizing center: detection of the DOD bending vibrations by means of Fourier transform infrared spectroscopy. Biochemistry. 2008;47:11024–30.
66. Noguchi T. Fourier transform infrared analysis of the photosynthetic oxygen-evolving center. Coord Chem Rev. 2008;252:336–46.
67. Siegbahn PE. A structure-consistent mechanism for dioxygen formation in photosystem II. Chem Eur J. 2008;14:8290–302.
68. Siegbahn PE. Structures and energetics for O_2 formation in photosystem II. Acc Chem Res. 2009;42:1871–80.
69. Gabdulkhakov A, Guskov A, Broser M, Kern J, Müh F, Saenger W, Zouni A. Probing the accessibility of the Mn_4Ca cluster in photosystem II: channels calculation, noble gas derivatization, and cocrystallization with DMSO. Structure. 2009;17:1223–34.
70. Ho FM, Styring S. Access channels and methanol binding site to the $CaMn_4$ cluster in Photosystem II based on solvent accessibility simulations, with implications for substrate water access. Biochim Biophys Acta. 2008;1777:140–53.
71. Murray JW, Barber J. Structural characteristics of channels and pathways in photosystem II including the identification of an oxygen channel. J Struct Biol. 2007;159:228–37.
72. Saito K, Shen JR, Ishida T, Ishikita H. Short hydrogen bond between redox-active Tyrosine Y_Z and D1-His190 in the photosystem II crystal structure. Biochemistry. 2011;50:9836–44.

73. Hays AMA, Vassiliev IR, Golbeck JH, Debus RJ. Role of D1-His190 in the proton-coupled oxidation of tyrosine Y_Z in manganese-depleted Photosystem II. Biochemistry. 1999;38:11851–65.
74. Hoganson CW, Babcock GT. A metalloradical mechanism for the generation of oxygen from water in photosynthesis. Science. 1997;277:1953–6.
75. Tommos C, Babcock GT. Proton and hydrogen currents in photosynthetic water oxidation. Biochim Biophys Acta. 2000;1458:199–219.
76. Kawakami K, Umena Y, Kamiya N, Shen JR. Location of chloride and its possible functions in oxygen-evolving photosystem II revealed by X-ray crystallography. Proc Natl Acad Sci U S A. 2009;106:8567–72.
77. Murray JW, Maghlaoui K, Kargul J, Ishida N, Lai TL, Rutherford AW, Sugiura M, Boussac A, Barber J. X-ray crystallography identifies two chloride binding sites in the oxygen evolving centre of Photosystem II. Energ Environ Sci. 2008;1:161–6.
78. Debus RJ. Protein ligation of the photosynthetic oxygen-evolving center. Coord Chem Rev. 2008;252:244–58.
79. Popelková H, Yocum CF. Current status of the role of Cl^- ion in the oxygen-evolving complex. Photosynth Res. 2007;93:111–21.
80. Wincencjusz H, van Gorkom HJ, Yocum CF. The photosynthetic oxygen evolving complex requires chloride for its redox state $S_2 \rightarrow S_3$ and $S_3 \rightarrow S_0$ transitions but not for $S_0 \rightarrow S_1$ or $S_1 \rightarrow S_2$ transitions. Biochemistry. 1997;36:3663–70.